Modelling lava flow advance using a shallow-depth approximation for three-dimensional cooling of viscoplastic flows

NOÉ BERNABEU[1,2], PIERRE SARAMITO[1]* & CLAUDE SMUTEK[2]

[1]*Laboratoire Jean Kuntzmann, UMR 5524 University J. Fourier – Grenoble I and CNRS, BP 53, F-38041 Grenoble cedex, France*

[2]*Laboratoire géosciences – IPGP and La Réunion University, 15, av. René Cassin, CS 92003, 97744 Saint-Denis cedex 09, France*

Corresponding author (e-mail: pierre.saramito@imag.fr)

Abstract: A new shallow-depth approximation model for lava flow advance and cooling on a quantized topography is presented in this paper. To apply the model, lava rheology is described using a non-isothermal three-dimensional viscoplastic fluid in which the rheological properties are assumed to be temperature dependent. Asymptotic analysis allows a three-dimensional flow scenario to be reduced to a two-dimensional problem using depth-averaged equations. These equations are numerically approximated by an autoadaptive finite element method, based on the Rheolef C++ library, which allows economy of computational time. Here, the proposed approach is first evaluated by comparing numerical output with non-isothermal experimental results for a flow of silicon oil. Finally, the December 2010 eruption of Piton de la Fournaise (La Réunion Island) is numerically reproduced and compared with available data.

More than 500 million people live near active volcanoes. It is thus essential to understand the risks presented by volcanic eruptions and to understand how to respond to an effusive emergency (Tilling 1989; Kusky 2008; Roult *et al.* 2012). In this regard, the purpose of lava flow simulation should be to forecast lava flow path with some degree of precision so as to protect the population (Hidaka *et al.* 2005; Cappello *et al.* 2010; Rongo *et al.* 2011). Lava flows are complex phenomena that combine non-Newtonian fluid dynamics and thermodynamics. Risk assessments for lava flows pose a difficult challenge for numerical modelling because they are three-dimensional thermo-mechanical entities with a free surface. The movement of lava can thus be approximated using fluid dynamic equations (such as Navier–Stokes) coupled with models that account for lava cooling as obtained from a thermal balance equation, which integrates the diffusion–convection in the lava, radiation and convection in the air, and conduction in the substrate (Wooster *et al.* 1997; Wright *et al.* 2000; Harris & Rowland 2009). Thus, to predict flow path, the simulation code must be faster than real-time flow, yet take into account all of these physical realities.

This paper describes a new robust and efficient numerical method that is based on asymptotic analysis. This approach is used to resolve the shallow-depth approximation for three-dimensional non-isothermal viscoplastic flow on a pre-described topography, while incorporating a temperature-dependent consistency index and yield strength

measure. The first section presents the three-dimensional problem, its two-dimensional surface and the numerical resolution of the associated equations. The second section provides validation for our approach based on comparisons between numerical simulation and experimental measurements performed using a flow of non-isothermal silicone oil. The third, and final, section develops (in detail) a comparison between our numerical predictions and real data obtained for the lava flow of December 2010 on Piton de la Fournaise.

Statement of the problem

To overcome the natural complexities inherent in lava flow modelling, some authors propose a probabilistic approach based on the topography. In these cases, the flow path is determined by the line of steepest descent, for example the DOWNFLOW (Tarquini & Favalli 2011) and ELFM (Damiani *et al.* 2006) codes. Such codes require a short computational time and minimal input data, which is an advantage. However, this approach cannot predict the spatial extent of flow through time, its thickness or its final emplacement. A deterministic approach results in a more constrained description of the phenomena. Harris & Rowland (2001) proposed a kinematic one-dimensional thermo-rheological model for lava flow in a confined channel (the FLOWGO code). In Hidaka *et al.* (2005), a three-dimensional model for a Newtonian fluid, which includes energy

conservation, solidification and free surface, was presented. A variant on the deterministic approach is the cellular automata method. This allows two-dimensional computation = based on spatial partition of mass and energy into cells whose state evolves according to that of their neighbours. Such models thus, also, involve a transition function that describes the exchanges of heat and mass between the lava control volume and its surroundings. Take, for example, the MAGFLOW code of Vicari *et al.* (2007) which evaluates = flow of a Bingham fluid on an inclined plane, or the SCIARA code of Spataro *et al.* (2010) which is based on a minimization rule based on the difference in height between neighbouring cells, while lava cooling takes into account radiation at the free surface and the heat exchange owing to lava mixing. We argue that such cellular automata methods cannot quantitatively predict the distribution of lava through time because such models do not solve the full suite of fluid dynamics-based equations.

Lava flows generally extend over several kilometres, although their thickness remain relatively small, being generally in the range of $1-10$ m, in regard to their length and width. An asymptotic analysis based on these aspect ratios allows the three-dimensional set of conservation laws and constitutive equations to be reduced to a two-dimensional system of equations. For inertia-dominated flows, we obtain the classical Saint-Venant shallow water model (Barré de Saint-Venant 1871), in which viscous terms are neglected. Gerbeau & Perthame (2001) proposed a modified Saint-Venant system in which viscous effects are maintained through a wall friction term. Costa & Macedonio (2005) extended this viscous variant by including non-isothermal and viscous heating effects for lava flows. Note that free surface viscoplastic lava flows are highly viscous and, thus, these inertia-dominated models could be improved. Huppert (1982) investigated Newtonian viscous flows. Rheological studies (e.g. Shaw 1969; McBirney & Murase 1984; Pinkerton & Norton 1995) indicated that lava flows are non-Newtonian and that the macroscopic flow can be described by a Bingham (1922) model, or (by its extension), the Herschel & Bulkley (1926) model, as shown in Figure 1. Shallow-flow approximations for a viscoplastic fluid flow in a horizontal dam break problem were first studied by Liu & Mei (1989) and revisited by Balmforth and Craster (Balmforth *et al.* 2006). Computations for specific three-dimensional topographies were next performed using specific axisymmetric coordinate systems using a curved channel (Mei & Yuhi 2001) and a conical surface (Yuhi & Mei 2004). Recently, an extension applicable to an arbitrary topography has been presented by the authors of this paper (Bernabeu *et al.* 2013). Taking cooling and

increase in viscosity and yield strength into account during cooling is more complex with the asymptotic analysis approach. That is, the problem does not reduce to a two-dimensional one, but remains fully three dimensional. To overcome this difficulty, different approaches based on a depth-average version of the heat equation were investigated by Bercovici & Lin (1996) for a Newtonian fluid so as to model the cooling of mantle plume heads with temperature-dependent buoyancy and viscosity. Balmforth and Craster then applied this approach to the evolution of a lava dome (Balmforth *et al.* 2004) for viscoplastic fluids with a temperature-dependent consistency index and yield strength.

Any computational model thus requires physical parameters of the lava to be input (as listed in Tables 1 & 2) and the three-dimensional topography to be well-defined, together with the location of events and their lava output rates. To build our shallow-depth averaged model, we thus made the following assumptions:

- (H1) flow can be described by viscoplastic Herschel–Bulkley behaviour;
- (H2) the flow is laminar;
- (H3) there is a thin film approximation;
- (H4) temperature can be modelled by a polynomial function in the vertical direction.

Assumption (H1) coupled with thermo-dependence of rheological parameters makes it possible to model cooling and stipping conditions. Assumptions (H2) and (H3) have generally been verified for lava flows (Balmforth *et al.* 2001). This knowledge thus allows the dynamic equations required to define
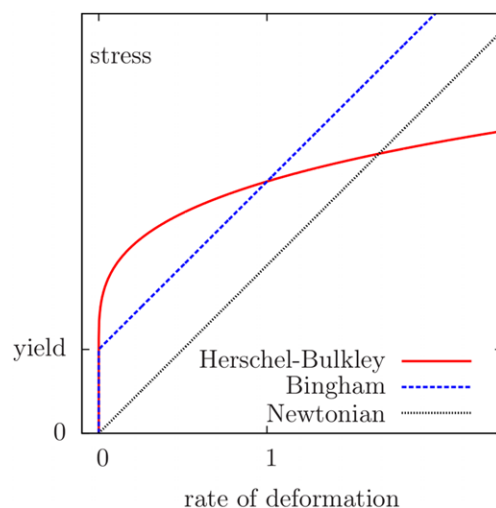

Fig. 1. Viscoplastic rheologies: shear-thinning and yield stress effects.

Table 1. *Physical parameters for the laboratory experiments (Garel* et al. *2012)*

Physical quantities	Symbol	Value	Unit
Experimental supply rate	Q	2.2×10^{-8}	$m^{-3} s^{-1}$
Initial temperature of the injected fluid	θ_e	315.15	K
Initial temperature of air and Polystyrene	θ_a	293.151	K
Fluid density	ρ	954	$kg\ m^{-3}$
Air density	ρ_a	1.2	$kg\ m^{-3}$
Herschel–Bulkley power index	n	1	–
Fluid viscosity at θ_e temperature	K_e	3.4	Pa s
Fluid emissivity	E	0.96	–
Thermal conductivity of the fluid	k	0.15	$W\ m^{-1}\ K^{-1}$
Fluid specific heat	C_p	1500	$J\ m^{-1}\ K^{-1}$
Convective heat transfer coefficient with air	λ	1–3	$W\ m^{-2}\ K^{-1}$
Thermal conductivity of the polystyrene	k_s	0.03	$W\ m^{-1}\ K^{-1}$
Thermal diffusivity of the polystyrene	κ_s	6×10^{-7}	$m^2\ s^{-1}$
Vent radius	r_e	2–4	mm
Constant in Arrhenius law (13)	α	8×10^{-3}	K^{-1}
Constant in Huppert (Huppert 1982) formula	a	0.715	dimensionless

the two-dimensional lava flow surface to be defined. Assumption (H4) is a closure equation necessary to reduce the heat-balance equation into a two-dimensional problem. This assumption is more debatable than the others, but it is mathematically the simplest way to reduce the heat equation into a solvable problem. In particular, it limits the need to model abrupt vertical temperature variations, and is more appropriate for very viscous (aa) than very thin (pahoehoe) lava flows. We aim to develop a more complex multilayer vertical temperature profile in the future. Here, though, we present a first polynomial approximation which, despite its limitations, produces interesting results.

Three-dimensional formulation

The viscoplastic Herschel–Bulkley constitutive equation (Herschel & Bulkley 1926) expresses the deviatoric part of the stress tensor versus the rate of deformation tensor $\dot{\gamma} = \nabla u + \nabla u^{\mathrm{T}}$. As a result, we can write:

$$\begin{cases} \tau = K(\theta)|\dot{\gamma}|^{n-1}\dot{\gamma} + \tau_y(\theta)\dfrac{\dot{\gamma}}{|\dot{\gamma}|} & \text{when } \dot{\gamma} \neq 0, \\ |\tau| \leq \tau_y & \text{otherwise.} \end{cases} \quad (1)$$

where u is the velocity field, θ is the temperature, $K(\theta) > 0$ is the temperature-dependent

Table 2. *Physical parameters for the lava flow*

Physical quantities	Symbol	Value	Unit
Average eruption flow rate	Q	9.7	$m^{-3} s^{-1}$
Eruption duration	d_e	15:15	h:min
Initial temperature of the fluid	θ_e	1423	K
Initial temperature of air and substrate	θ_a	303	K
Lava density	ρ	2200	$kg\ m^{-3}$
Air density	ρ_a	1.2	$kg\ m^{-3}$
Lava viscosity at θ_e temperature	K_e	10^4	Pa s
Lava yield stress at θ_e temperature	$\tau_{y,e}$	10^2	Pa s
Lava emissivity	E	0.95	–
Lava thermal conductivity	k	2	$W\ m^{-1}\ K^{-1}$
Lava specific heat	C_p	1225	$J\ m^{-1}\ K^{-1}$
Convective heat transfer coefficient with air	λ	80	$W\ m^{-2}\ K^{-1}$
Flow characteristic thickness	H	1	m
Flow characteristic length	L	1000	m
Constant in viscosity Arrhenius law	α	0.016	K^{-1}
Constant in yield stress Arrhenius law	β	0.116	K^{-1}

See Villeneuve *et al.* (2008), McBirney & Murase (1984), Pinkerton & Norton (1995), Shaw (1969) and Roult *et al.* (2012) for the 2010 eruption data.

consistency index, $n > 0$ is the power-law index and $\tau_y(\theta)$ is the temperature-dependent yield strength. The consistency index and the yield strength generally decrease with the temperature. Here $|\tau| = ((1/2) \sum_{i,j=1}^{3} \tau_{ij}^2)^{1/2}$ denotes the norm of a symmetric tensor, τ. The total Cauchy stress tensor can be described by $\sigma = -p.I + \tau$ where p is = pressure and I the identity tensor. When $\tau_y = 0$ and $n = 1$, the fluid is Newtonian; and K is viscosity. When $\tau_y = 0$ and $n > 0$ the fluid corresponds to a quasi-Newtonian power law. When $\tau_y > 0$ and $n = 1$, the model reduces to the Bingham (1922) law. Constitutive equation (1) should be supplemented by the mass, momentum and energy conservation laws, so that:

$$\text{div } u = 0 \tag{2}$$

$$\rho(\partial_t u + u.\nabla u) - \text{div}(-p.I + \tau) = \rho g \tag{3}$$

$$\rho C_p(\partial_t \theta + u.\nabla \theta) - \text{div}(k\nabla \theta) - \frac{\tau : \dot{\gamma}}{2} = 0. \tag{4}$$

where ρ is density, C_p is specific heat, k is thermal conductivity and g is gravity. Note that there are four equations (1–4) and four unknowns τ, $u = (u_x, u_y, u_z)$, p and θ. The problem can thus be solved by defining the boundary and initial conditions.

We consider a flow over a variable topography as erupted from a vent that feeds a flow that then undergoes cooling (see Fig. 2). For any time $t > 0$, the flow domain is represented by:

$$\Lambda(t) = \{(x, y, z) \in \Omega \times \mathbb{R};$$

$$f(x, y) < z < f(x, y) + h(t, x, y)\}$$

where Ω is an open and bounded subset $\mathbb{R}^2$. The function f denotes the topography and h is the flow height because the vent is described by an open subset Ω_e of Ω (see Fig. 2) and $\Omega_s = \Omega \backslash \bar{\Omega}_e$ denotes its complement. The boundary $\partial \Lambda(t)$ of the lava flow volume $\Lambda(t)$ can be split into three parts (see Fig. 2): the basal topography at the vent Γ_e, basal topography beyond the vent Γ_s and the flow (upper) free surface $\Gamma_f(t)$.

Also, $S = \{(x, y, z) \in \Omega_s \times \mathbb{R}; \quad z < f(x, y)\}$ denotes the substratum. For cases where $t > 0$, boundary conditions at the flow base are a non-slip condition on Γ_s (beyond the vent) and a vertical profile on Γ_e (in the vent) for the velocity field, and natural zero normal stress on the free surface:

$$u_x = u_y = 0 \quad \text{and} \quad u_z = w_e \quad \text{on} \quad \Gamma_e \cup \Gamma_s \tag{5}$$

$$\sigma.v_f = 0 \quad \text{on} \quad \Gamma_f(t) \tag{6}$$

where v_f denotes the unit outward vector of $\partial \Lambda(t)$ on $\Gamma_f(t)$. Here, w_e is the lava eruption velocity, defined as $]0, +\infty[\times \Gamma_e$, and satisfying $w_e \neq 0$ on Γ_e and $w_e = 0$ on Γ_s. For the temperature, an isothermal boundary condition at the vent, a conduction flux at the flow base to the flow substratum (beyond vent) and radiative and convection fluxes with air at the flow free surface are accounted for by:

$$\theta = \theta_e \quad \text{on} \quad \Gamma_e \tag{7}$$

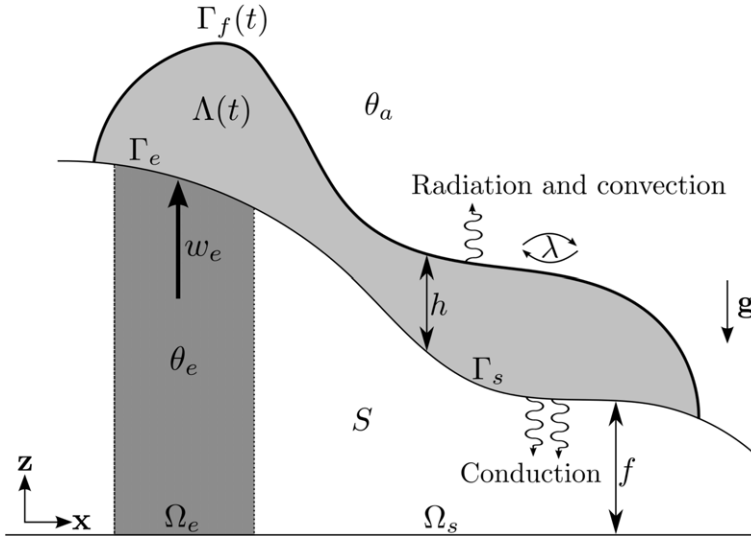$$k v_s.\nabla \theta = k_s v_s.\nabla \theta_s \quad \text{on} \quad \Gamma_s \tag{8}$$

Fig. 2. Lava flow erupted from a vent on a variable topography. The flow loses heat to the air through radiation and convection, and to the ground through conduction.
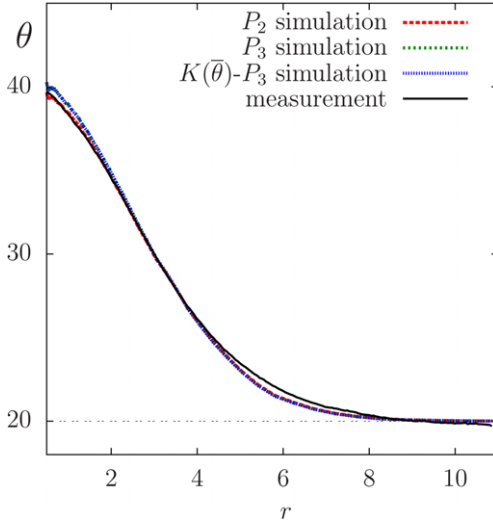
Fig. 3. Steady-state surface temperature $\theta(z = f + h)$ in °C v. radius r in cm at $t = 7480$ s and $\lambda = 2$ W m^{-2} K^{-1}. Comparison between different simulation variants and experimental measurments from Garel *et al.* (2012). The label P_2 is linked to a constant viscosity model similar to those of Bercovici and Lin (Bercovici & Lin 1996): the viscosity is set at its value at the eruption temperature K_e (see Table 1), the temperature profile $\theta = \varphi \bar{\theta}$ is approximated with a second-order polynomial φ in the vertical direction and the term $\text{div}(h(\overline{\varphi \mathbf{u}_{\|}} - \bar{\mathbf{u}}_{\|}))\bar{\theta}$ is ignored. The label P_3 denotes a constant viscosity model where φ is approximated by a third-order polynomial that satisfies $\overline{\varphi \mathbf{u}_{\|}} = \bar{\mathbf{u}}_{\|}$. Finally, the label $K(\bar{\theta}) - P_3$ denotes a non-constant viscosity model based on the Arrhenius law.

$$k\nu_f.\nabla\theta + E\,\sigma_{SB}(\theta^4 - \theta_a^4) + \lambda(\theta - \theta_a)$$
$$= 0 \quad \text{on} \quad \Gamma_f(t) \tag{9}$$

where θ_e is the initial eruption temperature, θ_s is the temperature of the substratum, θ_a is the temperature of the air, k_s is the thermal conductivity of the substratum, ν_s is the unit outward vector of $\partial\Lambda(t)$ on

Γ_s, $\in$ is the emissivity, σ_{SB} is the Stefan–Boltzman constant and λ is the convective heat transfer coefficient. Here, the term $k_s\nu_s.\nabla\theta_s$ represents the heat flux from the substratum (its derivation is described in Appendix A.1).

The free surface heat flux is described by $\Gamma_f(t)$, in which $z = f + h$, and heat is transported away from the flow surface by the u velocity field as described by the advection equation:

$$\partial_t h + u_x\partial_x(f + h) + \partial_y(f + h) = u_z \text{ in}]0, +\infty[\times \Omega \tag{10}$$

This is a first-order transport equation for the height h that should be supplemented by an initial condition:

$$h(t = 0, x, y) = h_{\text{init}}, \quad \forall(x, y) \in \Omega \tag{11}$$

in which h_{init} is given. The solution of this equation system is completed by definition of an initial condition for the velocity u and the temperature θ:

$$u(t = 0) = u_{\text{init}} \quad \text{and} \quad \theta(t = 0) = \theta_{\text{init}} \quad \text{in} \quad \Lambda(0). \tag{12}$$

To summarize, the three-dimensional problem requires the following input data: flow height h, the stress tensor τ, the velocity field u, pressure p and temperature θ. This allows us to solve equations (1)–(12). For lava flow applications, the finite element of finite difference discretizations of this problem led to a huge nonlinear and time-dependent set of equations. Appendix A presents a reduction to a two-dimensional problem.

Comparison with a silicone oil pancake experiment

Experimental setup and physical parameters

The evolution of lava domes was studied numerically by Balmforth and Craster using yield stress fluids (Balmforth *et al.* 2004). In 2012, Garel presented a laboratory experiment of a dome with silicone oil

Fig. 4. The Piton de la Fournaise December 2010 lava flow (credit N. Bernabeu, May 2014).
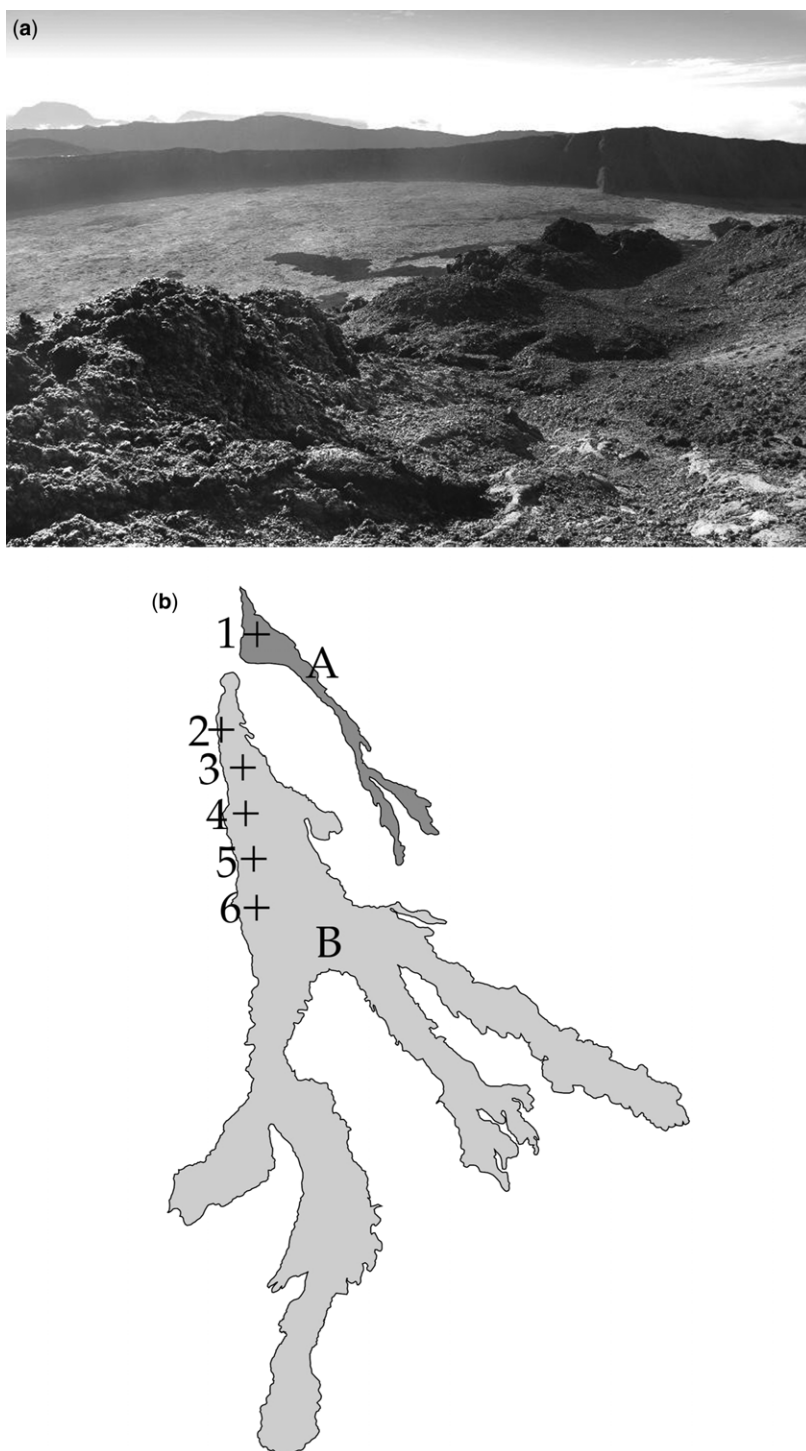
Fig. 5. (**a**) View of the aligned cones along the fault line associated with different vents (credit N. Bernabeu, 2014). (**b**) Schematic view of the different vent positions and the two separate zones of the observed flow's final emplacement.
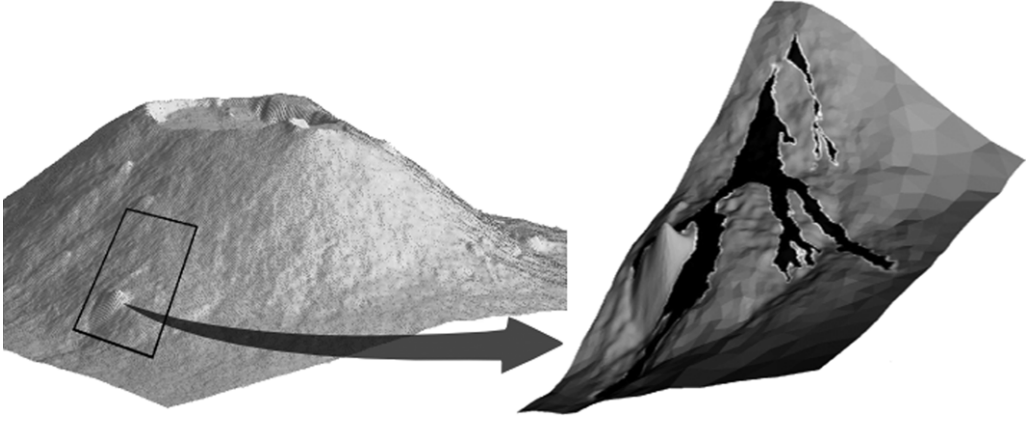
Fig. 6. Digital elevation model of the Piton de la Fournaise Volcano in 2008, with a 5 m horizontal resolution (left). Zoom of the observed flow's final emplacement (right). The dimensions of the rectangle are about 1700×1000 m.

(Newtonian fluid) that allowed surface temperature measurements (Garel *et al.* 2012). In this case, the fluid was supplied through a pipe (2 or 4 mm radius) along a horizontal plane at a constant supply rate Q. The fluid was initially heated to θ_e above the ambient temperature θ_a and a system of optical and infrared cameras was used to follow dome growth and surface temperature evolution. Table 1 details the relevant physical parameters used for this experiment. Fluid viscosity was measured for the full experimental temperature range, and data were first presented in Garel (2012, pp. 60–62). It should be observed that viscosity is here approximated by an Arrhenius law:

$$K(\theta) = K_e e^{\alpha(\theta_e - \theta)} \qquad (13)$$

where $\alpha = 8 10^{-3}$ K^{-1}, as obtained by a linear regression. The flow though the vent was intended to be a steady Poiseuille flow. Because the vent was circular with a radius of r_e, vertical velocity w_e is a second-order polynomial in relation to the radius. Thus: $w_e(r) = c \max(0, r_e^2 - r^2)$ where $c > 0$ is such that $\int_0^{r_e} w_e(r) r \, \mathrm{d}r = Q$, that is, $c = 2Q/(\pi r_e^4)$. Consequently, at time $t = 0$, fluid has not yet arrived on the flow-plane, so $h_{\text{init}} = 0$, u_{init} and θ_{init} do not need to be defined because $\Lambda(0) = \emptyset$.

Comparison between experiments and simulations

Figure 3 plots computed surface temperature as obtained by numerical simulations for different variants of our model. These simulations are also compared with experimental measurements from Garel *et al.* (2012): experiment C14. Note the

good ressemblance between all simulations and experimental data for this silicone oil lava flow. Results are very close for all model runs; the comparison is shown for time $t = 7480$ s, but this close relation is still valid for other times. In fact we find that a change from a P_2 to a P_3 model has little effect on numerical computations. The fact that a change from a P_3 to a $K(\bar{\theta}) - P_3$ model has little effect can be seen from the imperceptible difference between the two curves in Figure 3. Note that, in this experimental setup, viscosity varies by about a factor of 2 across a temperature range of 20 to 60 °C. Based on an autosimilar solution for the lava dome problem, Huppert (1982) proposed an explicit formula of the reference height h_{ref} and dome front radius $r_f(t)$ for the isothermal case:

$$h_{\text{ref}} = a \left(\frac{(\rho - \rho a) g Q^3}{3K} \right)^{1/4} \text{ and}$$

$$r_f(t) = a^{2/3} \left(\frac{3KQ}{(\rho - \rho_a) g} \right)^{1/8} t^{1/2} \qquad (14)$$

in which a is a constant and ρ_a is air density. Note that the viscosity K appears in (14) under $1/4$ and $1/8$ exponents: as a consequence, the dependence on temperature is negligible in the silicone oil flow evolution experience. This situation changes dramatically for real lava flows, as presented in the next section.

Comparison with a real lava flow

Description of the eruption

Piton de la Fournaise, a volcano on La Réunion Island, is among the most active volcanoes in the
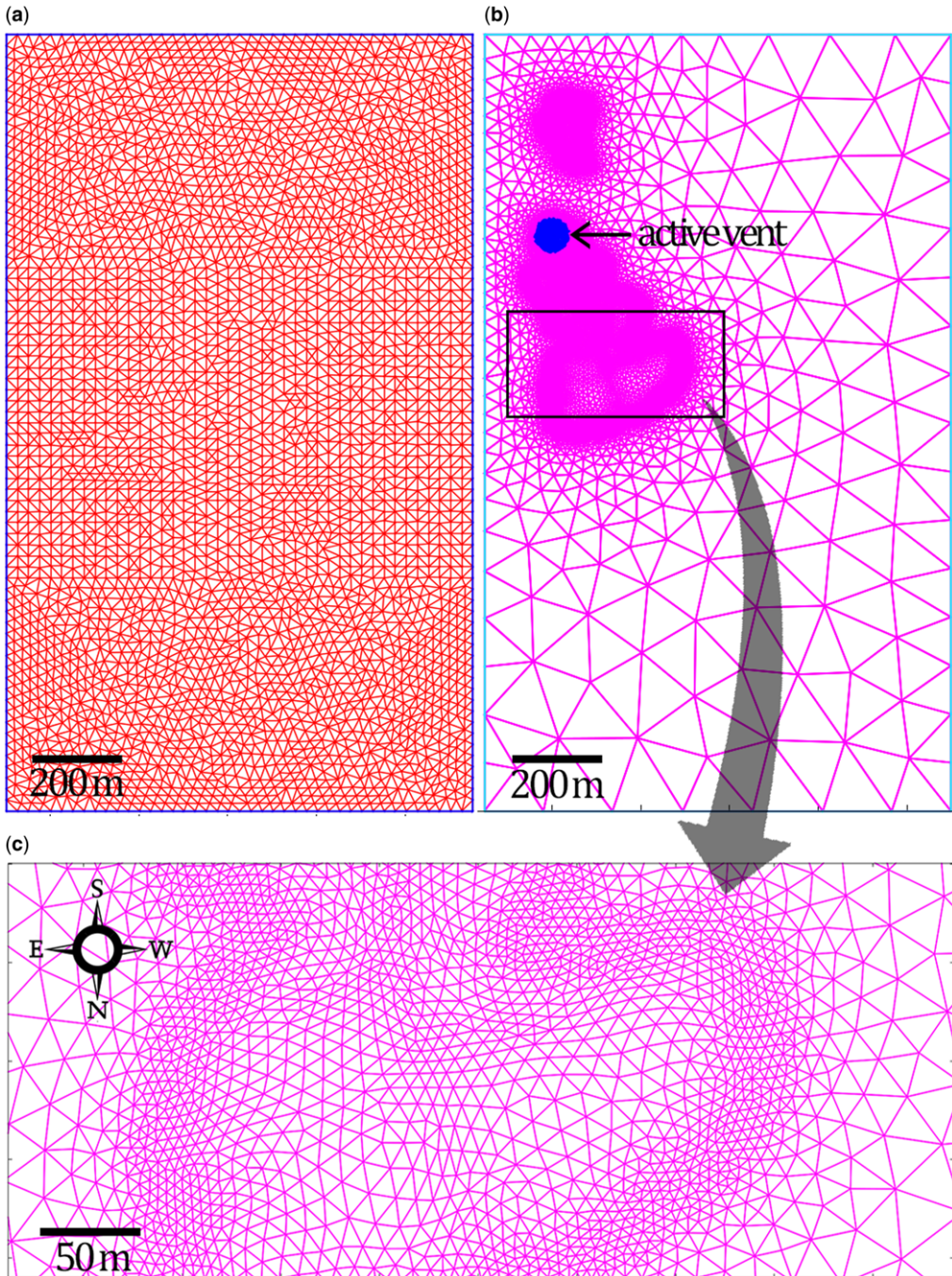
Fig. 7. Uniform (**a**) and dynamic (**b**) auto-adaptive meshes. Zoom near the front (**c**). This mesh was automatically generated for the lava flow simulation presented at $t = 5$ h.

world (see Roult *et al.* 2012). An effusive eruption occurred between the 9 and 10 December 2010 emplacing a lava flow on the north flank of the volcano. The duration of the eruption d_e is estimated as being 15 h 15 min, the average eruption flow rate Q was about 9.7 m^{-3} s^{-1}, the total erupted
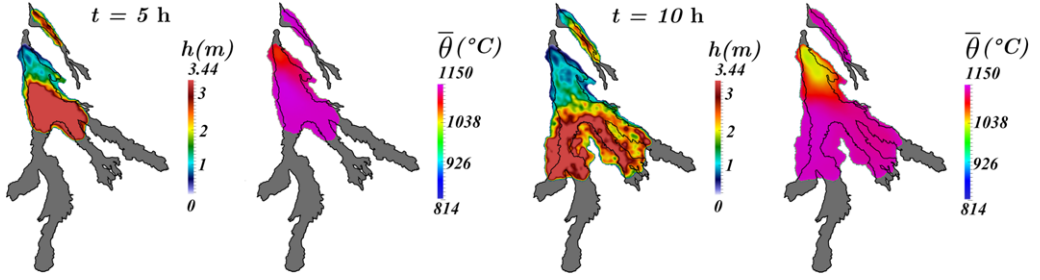
Fig. 8. Simulation of the lava flow after 5 and 10 h: (left) height h; (right) vertical-averaged temperature $\bar{\bar{\theta}}$. The contour of the real covered zone provided by the Volcano Observatory of Piton de la Fournaise is represented by a thin black line. Parameter values are given in Table 2.

volume was about $0.53 \times 10^6 \, \text{m}^3$ and the flow length was almost 2 km. These data were estimated by the Volcanological Observatory of Piton de la Fournaise as published in Roult *et al.* (2012). Figure 4 plots the final area of the lava flow field. Table 2 presents all of the relevant physical quantities for the simulation. The fluid is represented by a Bingham viscoplastic rheological model (with a power law index of $n = 1$). The substrate and the lava have similar properties, such as density and thermal conductivity, because the substrate is composed of old cooled lava of the same composition of the erupted volume. The consistency index and the yield strength depend on temperature and vary over a large range of magnitude. Here, we assume that fluid viscosity and the yield strength follow an Arrhenius law (Dragoni 1989): $K(\theta) = K_e e^{\alpha(\theta_e - \theta)}$ and $\tau_y(\theta) = \tau_{y,e} e^{\beta(\bar{\theta}_e - \theta)}$ in which $\alpha = \beta = 0.016 \, \text{K}^{-1}$. Finally, at time $t = 0$, the lava has not yet arrived on the cold ground, so $h_{\text{init}} = 0$, u_{init} and θ_{init} do not need to be defined because $\Lambda(0) = \emptyset$. Fieldwork was necessary to accurately locate the different vents (see Fig. 5a). Note on Figure 5b that the 2010 lava flow splits into two separate zones, denoted A and B, in which the different vents are numbered from 1 to 6.

Flow conditions and simulation parameters

The Volcano Observatory of Piton de la Fournaise (OVPF) provided us with a three-dimensional digital elevation model (DEM) of Piton de la Fournaise (horizontal resolution of 5 m) covering the zone of the new eruption (Fig. 6). Because this topographic survey predates 2010, it can be used to define the topography function f in our model. OVPF also provided us with the detailed contours for the final lava flow emplacement (see Fig. 6 right): this data is used for comparison with the numerical simulations. The flow rates of the two separate flows A and B (see Fig. 5b) are estimated as being proportional to their relative areas, that is, $Q_A = \kappa Q$ and $Q_B = (1 - \kappa)Q$, where $\kappa = |A|/(|A| + |B|)$ and $|A|$ and $|B|$ denote the areas of zones A and B, respectively. Note that these areas are calculated from the detailed contours of the lava flow field final emplacement area. In zone A, we assume that vent 1 is a circular cone with a radius of 20 m and is active throughout the whole period of eruption. In zone B, we assume that vents 2–6 are active consecutively and that they are circular. The eruption duration is denoted by d_e. We assume that vent 2 is active from $t = 0$ to $d_e/5$ with a radius of 10 m and vent i,
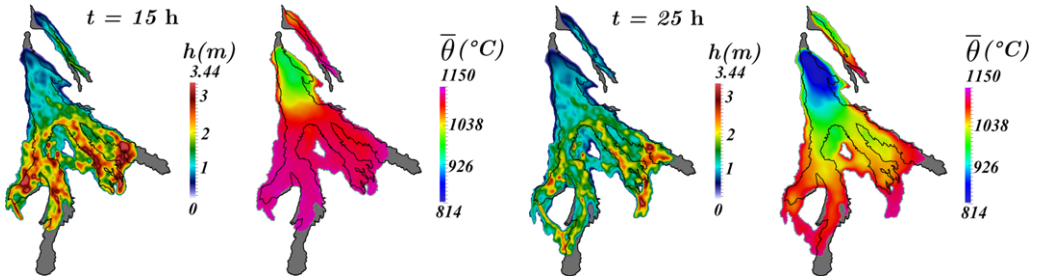

Fig. 9. Simulation of the lava flow after 15 and 25 h: (left) height h; (right) vertical-averaged temperature $\bar{\bar{\theta}}$. The contour of the real covered zone provided by the Volcano Observatory of Piton de la Fournaise is represented by a thin black line. Parameter values are given in Table 2.

$3 \leq i \leq 6$, is active from $t = (i - 2d_e/5)$ to $(i - 1)d_e/5$ with a radius of 20 m.

Results and discussion

Numerical simulations were performed on this lava flow field using the $K(\bar{\theta}) - P_3$ model to test the ability of our model to reproduce the final deposit. The details of the numerical algorithm are provided in the Appendix. The computational code is based on the general-purpose Rheolef finite element library (Saramito 2013). A mesh adaptation technique allows the front position to be determined, as shown in Figure 7. The minimal computational mesh size is chosen to be the same as the DEM resolution: that is, 5 m; and the maximal one is 150 m. This approach quantitatively increases the precision of our computations, as shown in Roquet *et al.* (2000) in the context of viscoplastic flows. We carried out many simulations using different values of K_e, $\tau_{y,e}$, α and β, and we present here an empirical choice that provides the best fit between the modelled and the actual lava area. We perform a

sensibility analysis on the values of K_e and $\tau_{y,e}$: multiplying or dividing one of them by a factor ten do not change the solution significantly. For α and β, sensitivity does not change much over a factor of about 100, because the flow is slowed or stopped by the viscoplasticity and subsequently cools. We also studied the influence of the distribution of the lava volume between the different vents during the eruption period, maintaining the same total lava volume and average flow rate. The choice presented here provides a good distribution of the lava volume between the main branches over the input topography. We ran simulations with more lava from vents 2, 3 and 4, but this led to too much lava to the NW. We also ran other simulations with more lava from vents 5 or 6, but this led to too much lava to the NE. Figures 8 and 9 plot the temporal evolution of flow advance and cooling for various times until the flow stops advancing. The arrested state is reached at $t = 25$ h and is represented in Figure 10, as overlain on the DEM. At approximately 10 h after the lava supply stopped, part of the hot lava continued to
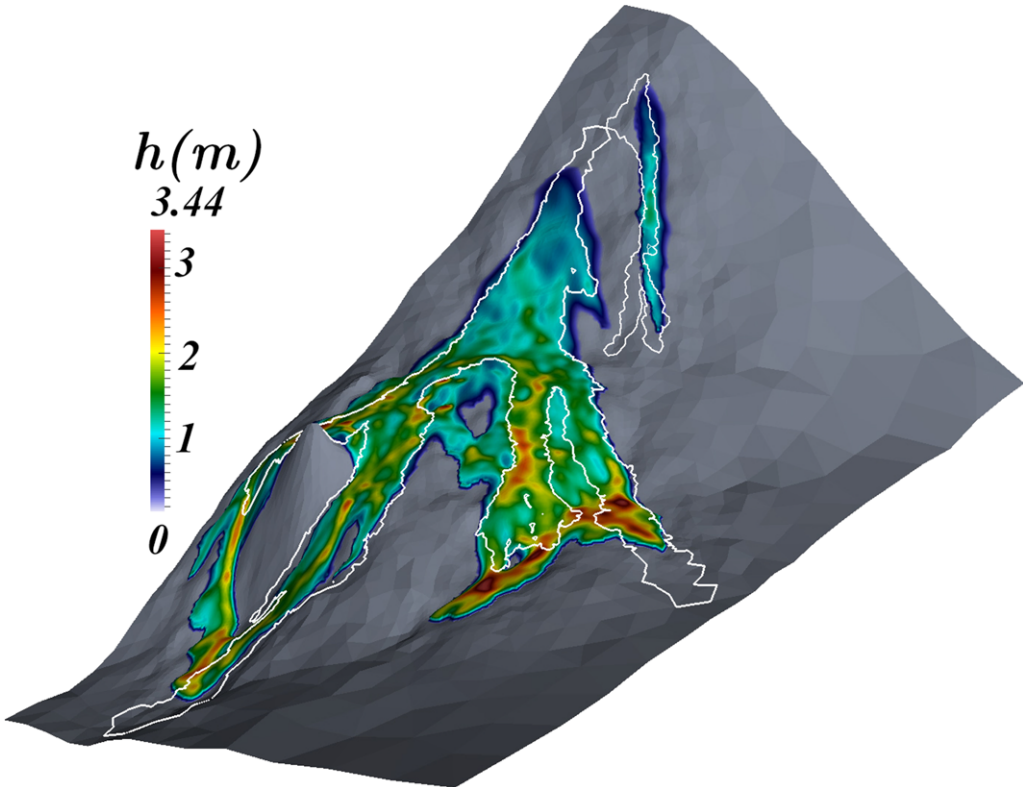

Fig. 10. Simulation of the lava flow: predicted flow final emplacement overlain onto the DEM with a colourmap showing the flow height h. The contour of the observed deposit zone provided by the Volcano Observatory of Piton de la Fournaise is represented by a thin white line.

flow and cool. Our model does not take into account solidification, so the final cessation of flow is due to the flow still being fluid enough to deform once supply has been cut. The value of the yield strength increases with cooling, and the flow stops once yield strength reaches strain rate (e.g. Hulme 1974). Note that the predicted flow-inundation zone is relatively close to that of the observed one, which is represented by a thin white line in Figure 10. Some discrepancies remain between the simulation and the observation: the final deposit is overestimated in certain places, the widths of the different flow branches are not always well predicted, and some flow bifurcations do not appear in the simulation. There are many possible explanations for these discrepancies. The main problem for the simulation was the lack of data concerning the 2010 lava flow, especially concerning the vent positions and their corresponding flow rates during the emission period. This missing data was estimated here, and we found that this slightly influenced the final results. A second source of error was the accuracy of the DEM used: its 5 m horizontal resolution can be related to the characteristic flow height of about 1 m. At this scale, a lot of ground detail is lost and a single block or a minor pre-existing topographical variation on the scale of 2 or 3 m can generate a bifurcation that would not be generated by the current DEM. A third source of error could be due to the model itself: vertical variation of the temperature is ignored here in the viscosity and the yield strength temperature-dependent functions, because only a vertically averaged temperature value is used. Future research directions could reconsider this vertical variation. Nevertheless, considering this lack of physical data, and our simplified shallow viscoplastic flow model, the numerical simulations are in relatively good agreement with the observations.

Conclusions

A new variant on the shallow-depth equation model for a flow of non-isothermal free-surface three-dimensional viscoplastic fluid over a generalized topography is presented. Both the consistency index and the yield strength are assumed to be temperature dependent. The governing equations were numerically approximated by an autoadaptive finite element method, allowing the flow front position to be tracked $=$. The proposed approach was evaluated by comparing numerical predictions with available data from both laboratory experiments using a non-isothermal silicone oil flow and real-world lava flows. These two tests showed that the numerical simulations are in relatively good

agreement with observations. Future work will use a new 1-m spatial resolution DEM of the Piton de la Fournaise Volcano to generate more accurate simulations, and will also explore lava flow simulations for other volcanoes. Another research direction is to improve our model by taking the vertical dependence of the temperature field into account in the viscosity and yield strength functions.

Appendix

A. The reduction model

A.1. Reduction to a two-dimensional problem. The asymptotic analysis approach developed here was initiated by Liu & Mei (1989) and then revisited by Balmforth and Craster (Balmforth *et al.* 2006) for an isothermal two-dimensional viscoplastic flow on a constant slope. Balmforth and Craster then extended this analysis to the non-isothermal case with axisymmetric geometry and applied it to a lava dome (Balmforth *et al.* 2004). In Bernabeu *et al.* (2013), the present authors extended this asymptotic analysis to the case of an isothermal three-dimensional viscoplastic flow on an arbitrarily topography. In the present paper, this analysis is extended to the case of a non-isothermal flow: the consistency index and the yield stress are assumed to be temperature-dependent.

For any function ψ of $]0, +\infty[\times Q(t)$, let us denote $\bar{\Psi}$ its vertical-averaged value, defined for all $(t, x, y) \in]0, +\infty[\times \Omega$ by

$$\bar{\Psi}(t, x, y) = \begin{cases} \dfrac{1}{h} \displaystyle\int_f^{f+h} \Psi(t, x, y, z)\, \mathrm{d}z & \text{when} \quad h \neq 0, \\ 0 & \text{otherwise.} \end{cases}$$

For simplicity, assume that the consistency index and the yield stress depend only on the vertical-averaged temperature: $K(\theta) = K(\bar{\theta})$ and $\tau_y(\theta) = \tau_y(\bar{\theta})$. This means that the effects of a vertical variation in temperature on the consistency index and the yield stress are ignored here, while their effects in the horizontal directions x and y are still taken into account. The problem is reformulated with dimensionless quantities and unknowns, denoted with tildes. The temperature is expressed as $\theta = \theta_a + (\theta_e - \theta_a)\bar{\theta}$. The temperature-dependent consistency index and yield stress are rescaled as $K(\theta) = K_e \tilde{K}(\tilde{\theta})$ and $\tau_y(\theta) = \tau_{y,}$

$e\tilde{\tau}_y(\tilde{\theta})$ where $K_e = K(\theta_e)$ and $\tau_{y,e} = \tau_y(\theta_e)$. Note that $\tilde{K}(1) = 1$ and $\tilde{\tau}_y(1) = 1$. Let H be a characteristic flow height and L be a characteristic horizontal length of the two-dimensional flow domain Ω. Let us introduce the dimensionless aspect ratio:

$$\varepsilon = \frac{H}{L}.$$

As in Huppert (1982), let $U = \rho g H^3/(\eta L)$ a characteristic flow velocity in the horizontal plane, where $\eta = K_e(U/H)^{n-1}$ is a characteristic viscosity and $g = |g|$ denotes the norm of gravity vector. The characteristic velocity can be expanded to

$$U = \left(\frac{\rho g H^2}{K_e L}\right)^{1/n} H.$$

Let $W = \varepsilon U$ be a characteristic velocity in the vertical direction, $T = L/U$ be a characteristic time and $P = \rho g H$ a characteristic pressure. We consider the following change in variables:

$$x = L\tilde{x}, \, y = L\tilde{y}, \, z = H\tilde{z}, \, t = T\tilde{t}, \, p = P\tilde{p}, \, h = H\tilde{h}$$
$$u_x = U\tilde{u}_x, \, u_y = U\tilde{u}_y, \, u_z = W\tilde{u}_z.$$

Note the non-isotropic scaling procedure for the vertical coordinate z and the vertical vector component u_z of the velocity vector. Hereafter, only the dimensionless problem is considered: for simplicity, and since there is no ambiguity, the tildes are omitted from the dimensionless variables. After the change in variables and an asymptotic analysis (see Bernabeu *et al.* (2013) for details of the isothermal case) the problem reduces to:

(P) find h and θ satisfying:

$$\partial_t h + \text{div}_{\|}(h\bar{u}_{\|}) = w_e \quad \text{in }]0, \, +\infty[\times \Omega \qquad (A1)$$

$$h(t = 0) = h_{\text{init}} \quad \text{in} \quad Q(0), \qquad (A2)$$

$$\frac{\partial(f + h)}{\partial n} = 0 \quad \text{in }]0, \, +\infty[\times \partial\Omega, \qquad (A3)$$

$$\partial_t \theta + u_x \partial_x \theta + u_y \partial_y \theta + u_z \partial_z \theta - \frac{1}{Pe} \partial_{zz} \theta = 0$$

$$\text{in }]0, \, +\infty[\times Q(t), \qquad (A4)$$

$$\theta(t = 0) = \theta_{\text{init}} \quad \text{in} \quad Q(0), \qquad (A5)$$

$$\frac{\partial\theta}{\partial z} + R p_\mu(\theta)\theta + Nu\theta = 0 \quad \text{on }]0, \, +\infty[\times \Gamma_f(t), \qquad (A6)$$

$$-\frac{\partial\theta}{\partial z} + \frac{\kappa_s}{\kappa}\left(\frac{Pe_s}{\pi t}\right)^{1/2}\theta = 0 \quad \text{on }]0, \, +\infty[\times \Gamma_s, \qquad (A7)$$

$$\theta = 1 \quad \text{on }]0, \, +\infty[\times \Gamma_e. \qquad (A8)$$

The problem involves six dimensionless numbers:

$$Bi = \frac{\tau_{y,e} H}{\eta U} \qquad \text{the Bingham number}$$

$$Pe = \frac{\rho C_p U L}{\kappa} \qquad \text{the Péclet number}$$

$$Pe_s = \frac{\rho_s C_{p,s} U L}{\kappa_s} \qquad \begin{array}{l}\text{the Péclet number in} \\ \text{the substrate}\end{array}$$

$$Nu = \frac{\lambda H}{\kappa} \qquad \text{the Nüsselt number}$$

$$R = \frac{H E \sigma_{SB}(\theta_e - \theta_a)^3}{\kappa} \qquad \text{a radiation number}$$

$$\mu = \frac{\theta_a}{\theta_e - \theta_a} \qquad \begin{array}{l}\text{a temperature ratio number,} \\ \text{for radiation}\end{array}$$

where Bi compares yield stress $\tau_{y,e}$ with a characteristic viscous stress $\eta U/H$ assumed to be $\mathcal{O}(1)$ in ε, Pe compares convection with diffusion and is assumed to be $\mathcal{O}(\varepsilon^{-2})$ and R and Nu in $\mathcal{O}(1)$ in ε and which represent the importance of radiative and convective transfer with air. Also, $p_\mu(\theta) = \theta^3 + 4\mu\theta^2 + 6\mu^2\theta + 4\mu^3$ for any $\theta \geq 0$. Note that problem (P) involves only h and θ: the velocity components $u_{\|} = (u_x, u_y)$ and u_z then involve explicit expressions using h and $\bar{\theta}$:

$$u_{\|} = \begin{cases} \dfrac{n}{n+1}|\nabla_{\|}(f + h)|^{1/n}\text{dir}(\nabla_{\|}(f + h))K^{-1}(\bar{\theta}) \\ [(f + h_c(\bar{\theta}) - z)^{1+1/n} - h_c^{1+1/n}] \\ \quad \text{when} \quad z \in [f, f + h_c(\bar{\theta})], \\ -\dfrac{n}{n+1}|\nabla_{\|}(f + h)|^{1/n}\text{dir}(\nabla_{\|}(f + h))K^{-1}(\bar{\theta})h_c^{1+1/n} \\ \quad \text{when} \quad z \in \,]f + h_c(\bar{\theta}), f + h[\end{cases}$$

and

$$u_z(t, x, y, z) = w_e - \int_f^z \text{div}_{\|}(u_{\|})\,\text{d}z$$

where

$$h_c(t, x, y) = \max\left(0, h - \frac{Bi\tau_y(\bar{\theta})}{|\nabla_{\|}(f + h)|}\right).$$

For convenience, we also denote the direction of any non-zero plane vector as $\text{dir}(v_{\|}) = v_{\|}/|v_{\|}|$. In equation (A7), the heat flux from the substratum has been estimated as in Garel *et al.* (2012, p. 6), thanks to an autosimilar solution for the temperature in the substratum $\theta_s(t, z)$ given in Carslaw & Jaeger (1946, p. 53). This approach leads to an explicit expression of θ_s v. θ and we then obtain a boundary condition in terms of θ alone.

A.2. Reduction of the heat equation. Note that the reduced problem still remains three dimensional, as equation (A4) is still defined on the three-dimensional flow domain $Q(t)$. This equation then needs to be integrated in the vertical direction and the problem expressed in terms of the averaged temperature $\bar{\theta}$. For any $t > 0$ and $(x, y) \in \Omega$, the heat equation (A4) is integrated from $z = f(t, x, y)$ to $z = f(t, x, y) + h(t, x, y)$. Then, using

equation (A1) and div $\mathbf{u} = 0$ leads to:

$$h\partial_t\bar{\theta} + div(h\bar{\theta}\mathbf{u}_{||}) - div(h\bar{\mathbf{u}}_{||})\bar{\theta} - w_e(1-\bar{\theta})$$

$$-\frac{1}{Pe}[\partial_z\theta(z=f+h) - \partial_z\theta(z=f)] = 0. \quad (A9)$$

In order to obtain a well-resolved problem in terms of $\bar{\theta}$ instead of θ, an additional relation should be introduced: the so-called closure relation, that expresses θ v. $\bar{\theta}$. A vertical profile θ is chosen according to $\bar{\theta}$ as $\theta(t,x,y,z) = \varphi(t,x,y,z)\bar{\theta}(t,x,y)$ where φ is an unknown function satisfying $\overline{\varphi} = 1$ and the boundary conditions in the vertical direction:

$$\partial_z\varphi + Rp_\mu(\bar{\theta}\varphi)\varphi + Nu\varphi = 0 \quad \text{on} \quad \Gamma_f(t),$$

$$-\partial_z\varphi + \frac{k_s}{k}\left(\frac{Pe_s}{\pi t}\right)^{1/2}\varphi = 0 \quad \text{on} \quad \Gamma_s \quad \text{and} \quad \overline{\theta}\varphi = 1 \quad \text{on} \quad \Gamma_e.$$

With these notations, (A9) becomes:

$$h(\partial_t\bar{\theta} + \overline{\varphi\mathbf{u}_{||}} \cdot \nabla\bar{\theta}) + div(h(\overline{\varphi\mathbf{u}_{||}} - \bar{\mathbf{u}}_{||}))\bar{\theta} - w_e(1-\bar{\theta})$$

$$-\frac{1}{Pe}[\partial_z\varphi(z=f+h) - \partial_z\varphi(z=f)]\bar{\theta} = 0. \quad (A10)$$

Note that $\overline{\varphi\mathbf{u}_{||}}$ corresponds to a weighted averaged velocity. The closure equation (A10) was first introduced by Bercovici & Lin (1996) in the context of cooling mantle plume heads: these authors showed that restricting $\varphi(t,x,y,z)$ to be a second-degree polynomial in z for any fixed (t,x,y) leads to a well-resolved reduced problem when replacing equation (A4) by equation (A10) in problem (P). Moreover, the computation of the φ polynomial coefficient at any (t,x,y) is easy and explicit. However, this second-order polynomial approximation in z does not allow the term $div(h(\overline{\varphi\mathbf{u}_{||}} - \bar{\mathbf{u}}_{||}))\bar{\theta}$ to be eliminated from equation (A10). There is also no evidence that it is always positive: it can thus generate exponential growth of the averaging temperature, which is difficult to handle in a numerical simulation. Finally, the physical meaning of this term is unclear and Bercovici and Lin neglected $div(h(\overline{\varphi\mathbf{u}_{||}} - \bar{\mathbf{u}}_{||}))\bar{\theta}$ in the previous equation. These authors showed that a real numerical error is committed when based on this hypothesis: the order of error is of about 10% for their specific problem (Bercovici & Lin 1996, p. 3307). Note that, while a 10% error is acceptable for some applications (such as volcanology, since input parameters are not generally known to such a level of accuracy), nevertheless, from a mathematical point of view, all convergence properties v. ε are definitively lost.

In the present paper, we propose a variant of this approach that conserves the convergence properties v. ε: we choose φ as a third-degree polynomial in z. This choice allows one additional degree of freedom at each (t,x,y) and we choose to impose a value of $\overline{\varphi\mathbf{u}_{||}} = \bar{\mathbf{u}}_{||}$ at any (t,x,y) as an additional constraint. Let (t,x,y) be fixed and $\varphi(z) = az^3 + bz^2 + cz + d$: then the four unknown

coefficients a, b, c and d comprise the only solution of the following four equations:

$$\overline{\varphi} = 1 \quad (A11)$$

$$\overline{\varphi\mathbf{u}_{||}} - \bar{\mathbf{u}}_{||} = 0 \quad (A12)$$

$$\frac{\partial\varphi}{\partial z} + (Rp_\mu(\bar{\theta}\varphi) + Nu)\varphi = 0 \quad \text{on} \quad z = f+h \quad (A13)$$

$$-\frac{\partial\varphi}{\partial z} + \frac{\kappa_s}{\kappa}\left(\frac{Pe_s}{\pi t}\right)^{\frac{1}{2}}\varphi = 0 \quad \text{on} \quad \Gamma_s \quad \text{and}$$

$$\bar{\theta}\varphi = 1 \quad \text{on} \quad \Gamma_e, \quad \text{on} \quad z = f. \quad (A14)$$

The reduced problem is then obtained from (P) by replacing (A4) by

$$h(\partial_t\bar{\theta} + \bar{\mathbf{u}}_{||}.\nabla\bar{\theta}) - w_e(1-\bar{\theta}) - \left(\frac{3ah^2 + 2bh}{Pe}\right)\bar{\theta} = 0 \quad (A15)$$

and the initial and boundary conditions (A5)–(A8) by

$$\bar{\theta}(t=0) = \bar{\theta}_{\text{init}} \quad \text{on} \quad \Omega, \quad (A16)$$

$$\frac{\partial\bar{\theta}}{\partial n} = 0 \quad \text{on} \quad]0, +\infty[\times \partial\Omega. \quad (A17)$$

A.3. Numerical resolution. The nonlinear reduced problem in h and $\bar{\theta}$ is first discretized v. time by an implicit second-order variable step finite difference scheme (see Bernabeu *et al.* 2013). It leads to a sequence of nonlinear sub-problems in h_m and $\bar{\theta}_m$ that depends on the horizontal coordinates $(x,y) \in \Omega$ alone, where h_m and $\bar{\theta}_m$ are respectively approximations of h and $\bar{\theta}_m$ at a discrete time t_m. An under-relaxed fixed point algorithm is used for solving these nonlinear subproblems: it allows the parabolic evolution equation evolution, in terms of h_m, and the averaged heat equation, in terms of $\bar{\theta}_m$, to be decoupled. These equations are then discretized by an autoadaptive finite element method: the practical implementation is based on the Rheolef finite element library (Saramito 2013). This autoadaptive mesh method was first introduced in Saramito & Roquet (2001) for viscoplastic flows and then extended in Roquet & Saramito (2003); see these articles for the implementation details. The procedure is based on a mesh adaptation loop at each time step: your goal is to accurately catch the front's evolution, where $h = 0$ (see Fig. 7). At the front, both the h and $\bar{\theta}$ gradients are sharp. As the time approximation is a second-order one, the adaptation criterion c also takes into account the solutions at two previous time steps: $c = h_{m+1} + h_m + h_{m-1}$. The auto-adaptive mesh procedure requires the minimal and maximal mesh sizes together with the criterion. In Roquet *et al.* (2000), the benefit of using auto-adaptive meshes was theoretically investigated and also quantified for practical computations with viscoplastic fluids and compared with fixed mesh computations.

References

BALMFORTH, N.J., BURBIDGE, A.S. & CRASTER, R.V. 2001. Shallow Lava Theory. *Geomorphological Fluid Mechanics*, **582**, 164–187.

BALMFORTH, N.J., CRASTER, R.V. & SASSI, R. 2004. Dynamics of cooling viscoplastic domes. *Journal of Fluid Mechanics*, **499**, 149–182.

BALMFORTH, N.J., CRASTER, R.V., RUST, A.C. & SASSI, R. 2006. Viscoplastic flow over an inclined surface. *Journal of Non-Newtonian Fluid Mechanics*, **139**, 103–127.

BARRÉ DE SAINT-VENANT, A.J.C. 1871. Théorie et équations générales du mouvement non permanent des eaux courantes. *Comptes Rendus des séances de l'Académie des Sciences, Paris, France, Séance 17*, **73**, 147–154.

BERCOVICI, D. & LIN, J. 1996. A gravity current model of cooling mantle plume heads with temperature-dependent buoyancy and viscosity. *Journal of Geophysical Research*, **101**, 3291–3309.

BERNABEU, N., SARAMITO, P. & SMUTEK, C. 2013. Numerical modeling of non-newtonian viscoplastic flows: part II. Viscoplastic fluids and general tridimensional topographies. *International Journal of Numerical Analysis and Modeling*, **11**, 213–228.

BINGHAM, E.C. 1922. *Fluidity and Plasticity*. McGraw–Hill, New York.

CAPPELLO, Â.A., DEL NEGRO, C. & VICARI, A. 2010. Lava flow susceptibility map of Mt Etna based on numerical simulations. From physics to control through an emergent view. *World Scientific Series on Nonlinear Science B*, **5**, 201–206.

CARSLAW, H.S. & JAEGER, J.C. 1946. *Conduction of Heat in Solids*, 2nd edn. Oxford University Press, Oxford.

COSTA, A. & MACEDONIO, G. 2005. Numerical simulation of lava flows based on depth-averaged equations. *Geophysical Research Letters*, **32**, 2005.

DAMIANI, M.L., GROPPELLI, G., NORINI, G., BERTINO, E., GIGLIUTO, A. & NUCITA, A. 2006. A lava flow simulation model for the development of volcanic hazard maps for mount Etna (Italy). *Computers & Geosciences*, **32**, 512–526.

DRAGONI, M. 1989. A dynamical model of lava flows cooling by radiation. *Bulletin of Volcanology*, **51**, 88–95.

GAREL, F. 2012. *Modélisation de la dynamique et du refroidissement des coulées de lave: utilisation de la télédétection thermique dans la gestion d'une éruption effusive*. PhD thesis, Institut de physique du globe, Paris.

GAREL, F., KAMINSKI, E., TAIT, S. & LIMARE, A. 2012. An experimental study of the surface thermal signature of hot subaerial isoviscous gravity currents: implications for thermal monitoring of lava flows and domes. *Journal of Geophysical Research*, **117**, B02205.

GERBEAU, J.-F. & PERTHAME, B. 2001. Derivation of viscous Saint-Venant system for laminar shallow water; numerical validation. *Discrete and Continuous Dynamical Systems – Series B*, **1**: 89–102.

HARRIS, A.J. & ROWLAND, S. 2001. FLOWGO: a kinematic thermo-rheological model for lava flowing in a channel. *Bulletin of Volcanology*, **63**, 20–44.

HARRIS, A.J. & ROWLAND, S. 2009. Effusion rate controls on lava flow length and the role of heat loss: a review. *Studies in Volcanology: the Legacy of George Walker*. The Geological Society, London, Special Publications of IAVCEI, **2**, 33–51.

HERSCHEL, W.H. & BULKLEY, T. 1926. Measurement of consistency as applied to rubber-benzene solutions. *Proceedings of the American Society for Testing and Materials*, **26**, 621–633.

HIDAKA, M., GOTO, A., UMINO, S. & FUJITA, E. 2005. VTFS project: development of the lava flow simulation code LavaSIM with a model for three-dimensional convection, spreading, and solidification. *Geochemistry, Geophysics, Geosystems*, **6**, Q07008.

HUPPERT, H.E. 1982. The propagation of two-dimensional and axisymmetric viscous gravity currents over a rigid horizontal surface. *Journal of Fluid Mechanics*, **121**, 43–58.

KUSKY, T.M. 2008. *Volcanoes*. Infobase Publishing, **XV**.

LIU, K.F. & MEI, C.C. 1989. Slow spreading of a sheet of Bingham fluid on an inclined plane. *Journal of Fluid Mechanics*, **207**, 505–529.

MCBIRNEY, A.R. & MURASE, T. 1984. Rheological properties of magmas. *Annual Reviews on Earth and Planetary Science*, **12**, 337–357.

MEI, C.C. & YUHI, M. 2001. Slow flow of a Bingham fluid in a shallow channel of finite width. *Journal of Fluid Mechanics*, **431**, 135–159.

PINKERTON, H. & NORTON, G. 1995. Rheological properties of basaltic lavas at sub-liquidus temperatures: laboratory and field measurements on lavas from mount Etna. *Journal of Volcanology and Geothermal Research*, **68**, 307–323.

RONGO, R., AVOLIO, M.A. *ET AL.* 2011. Defining high-detail hazard maps by a cellular automata approach: application to Mount Etna (Italy). *Annals of Geophysics*, **Special Issue: V3-LAVA PROJECT**, 568–578.

ROQUET, N. & SARAMITO, P. 2003. An adaptive finite element method for Bingham fluid flows around a cylinder. *Computational Methods and Applied Mechanical Engineering*, **192**, 3317–3341.

ROQUET, N., MICHEL, R. & SARAMITO, P. 2000. Errors estimate for a viscoplastic fluid by using Pk finite elements and adaptive meshes. *Comptes Rendus des séances de l'Académie des Sciences, Paris, France, Séries 1*, **331**, 563–568, http://www-ljk.imag.fr/membres/Pierre.Saramito/cr2000.pdf

ROULT, G., PELTIER, A., TAISNE, B., STAUDACHER, T., FERRAZZINI, V. & DI MURO, A. 2012. A new comprehensive classification of the Piton de la Fournaise activity spanning the 1985–2010 period. Search and analysis of short-term precursors from a broad-band seismological station. *Journal of Volcanology and Geothermal Research*, **241**, 78–104.

SARAMITO, P. 2013. *Efficient C++ finite element computing with Rheolef*. CNRS and LJK, http://cel.archives-ouvertes.fr/cel-00573970. http://cel.archives-ouvertes.fr/cel-00573970

SARAMITO, P. & ROQUET, N. 2001. An adaptive finite element method for viscoplastic fluid flows in pipes. *Computational Methods and Applied Mechanical Engineering*, **190**, 5391–5412.

SHAW, H.R. 1969. Rheology of basalt in the melting range. *Journal of Petrology*, **10**, 510–535.

SPATARO, W., AVOLIO, M.V., LUPIANO, V., TRUNFIO, G.A., RONGO, R. & D'AMBROSIO, D. 2010. The latest release of the lava flows simulation model SCIARA: first application to mt Etna (Italy) and solution of the anisotropic flow direction problem on an ideal surface. *Procedia Computer Science*, **1**, 17–26.

TARQUINI, S. & FAVALLI, M. 2011. Mapping and DOWNFLOW simulation of recent lava flow fields at mount Etna. *Journal of Volcanology and Geothermal Research*, **204**, 27–39.

TILLING, R.I. 1989. Volcanic hazards and their mitigation: progress and problems. *Reviews of Geophysics*, **27**, 237–269.

VICARI, A., ALEXIS, H., DEL NEGRO, C., COLTELLI, M., MARSELLA, M. & PROIETTI, C. 2007. Modeling of the 2001 lava flow at Etna volcano by a cellular automata approach. *Environment Modeling and Software*, **22**, 1465–1471.

VILLENEUVE, N., NEUVILLE, D.R., BOIVIN, P., BACHELERY, P. & RICHET, P. 2008. Magma crystallization and viscosity: a study of molten basalts from the Piton de la Fournaise volcano (La Réunion island). *Chemical Geology*, **256**, 242–251.

WOOSTER, M.J., WRIGHT, R., BLAKE, S. & ROTHERY, D.A. 1997. Cooling mechanisms and an approximate thermal budget for the 1991–1993 Mount Etna lava flow. *Geophysical Research Letters*, **24**, 3277–3280.

WRIGHT, R., ROTHERY, D.A., BLAKE, S. & PIERI, D.C. 2000. Improved remote sensing estimates of lava flow cooling: a case study of the 1991–1993 Mount Etna eruption. *Journal of Geophysical Research: Solid Earth*, **105**(B10), 23681–23694.

YUHI, M. & MEI, C.C. 2004. Slow spreading of fluid mud over a conical surface. *Journal of Fluid Mechanics*, **519**, 337–358.